X-ray-excited optical luminescence and X-ray absorption fine-structures studies of CdWO$_4$ scintillator

S. M. V. Novais, M. E. G. Valerio and Z. S. Macedo*

Laboratory of Advanced Ceramic Materials, Physics Department, Federal University of Sergipe, 49.100-000 São Cristóvão, SE, Brazil. E-mail: zelia.macedo@gmail.com

X-ray-excited optical luminescence (XEOL) emission and excitation spectra as well as the EXAFS signal of CdWO$_4$ were measured in the energy region of the Cd and W absorption edges. From EXAFS refinement, structural parameters such as number of atoms, distance from the absorbing atom and width of coordination shells in the W neighborhood were determined. The role of W–O interactions on the intrinsic luminescence of CdWO$_4$ is discussed. The efficiencies of conversion, transfer and emission processes involved in the scintillation mechanism showed to be high when self-trapped excitons are formed locally by direct excitation of W ions. Annihilation of these excitons provides the characteristic scintillation of CdWO$_4$, a broad band emission with maximum at 500 nm. The presence of two energetically different O positions in the lattice gives rise to the composite structure of the luminescence band, and no influence of extrinsic defects was noticed. A mismatch between the X-ray absorption coefficient and the zero-order luminescence curves corroborates that the direct excitation of Cd ions induces secondary electronic excitations not very effective in transferring energy to the luminescent group, WO$_6$.

Keywords: CdWO$_4$; scintillators; EXAFS; XEOL.

1. Introduction

Scintillators are luminescent materials that efficiently absorb high-energy photons and then convert the absorbed radiation into visible light. In practical applications the scintillator is the primary radiation sensor. The emitted light is detected by photomultipliers or photodiodes to be converted into electrical signals (Greskovich & Duclos, 1997; Blasse, 1994). Cadmium tungstate (CdWO$_4$) is a well known scintillator with high detection efficiency for X- and γ-rays. CdWO$_4$ crystallizes in the wolframite structure with monoclinic symmetry belonging to the space group $P2/c$. In view of its chemical stability, non-hygroscopic nature and high density, CdWO$_4$ is a suitable material for several applications in medical physics and industry (Burachas et al., 1996; Sabharwal & Sangeeta, 1999).

At room temperature the optical absorption edge of CdWO$_4$ is near 325 nm (3.8 eV) and the crystal shows a strong blue–green emission under excitation with energies above the band gap. Such intrinsic emission is commonly ascribed to annihilation of a self-trapped exciton, which forms excited WO$_6^{6-}$ complexes (Lammers et al., 1981; Chirila et al., 2000a; Nagirnyi et al., 2003). A complete description of the creation of these self-trapped excitons is not well known at the moment, since they can result from electronic transitions between oxygen and tungsten orbitals but can also be created from the trapping of non-correlated pairs that interact to form trapped excitons (Nagirnyi et al., 2001; Pankratov et al., 2001). Investigations of the luminescence spectrum of CdWO$_4$ in excitation mode have been reported for photon energies in the range of the oxygen absorption edge, but no evidence of a direct dependence of the light output and the absorption coefficient of this element was observed (Nagirnyi et al., 2001). Additionally, no reports have been made, up to now, on the separate contributions of Cd and W core-level absorptions to the scintillation of CdWO$_4$. In the present work we have used synchrotron radiation in the energy range of the absorption edges of these cations to investigate the optical as well as the structural properties of CdWO$_4$.

One of the techniques used in our investigations was X-ray-excited optical luminescence (XEOL), which can be defined as the optical luminescence emitted following atomic core-level X-ray excitation (Soderholm et al., 1998). The use of synchrotron radiation as excitation source provides tunable X-ray photons, allowing the preferential excitation of the elements at energies near their absorption edges. The X-ray photons can excite core electrons to bound, quasi-bound or continuum states, allowing more pathways for a system to optically decay depending on the excitation channel and the nature of the material (Ko et al., 2010; Liu et al., 2010). The

XEOL process begins with the atom with an ionized inner shell relaxing either by emitting a photon (X-ray fluorescence) or generating a secondary electron (Auger effect). Such products can cause a secondary ionization and so on, giving rise to an avalanche of electrons and holes. The cascade process continues until the generated photons and electrons are unable to create further ionization (Rodnyi, 1997). Then, charge carriers are thermalized such that electrons move to the bottom of the conduction band whereas holes move to the top of the valence band. At this stage, many trapping processes can occur but ultimately the XEOL emission is obtained from electron–hole radiative recombination and the way this recombination happens defines the three main properties of the scintillation, namely emission spectra, luminescence lifetime and efficiency. The XEOL technique, for this reason, is very useful for understanding the whole process involved in the scintillation emission of a particular material.

Another important technique used in the present work was extended X-ray absorption fine structure (EXAFS), which is a useful tool to determine the arrangement of atoms in the neighborhood of the absorbing atom (Stern, 1988). EXAFS was used herein to investigate the local order surrounding the W ions and to confirm the length of the W—O bonds in the $CdWO_4$ structure. The possible relationship between the absorption coefficient of either Cd or W atom and the light output of the crystal was investigated by comparison of EXAFS spectra and XEOL, thus bringing some additional information for the full knowledge of the luminescent mechanism of this scintillator.

2. Experimental

Solid-state reaction was the synthesis route employed to produce $CdWO_4$ polycrystalline samples. Details about the production and structural characterization by X-ray diffraction (XRD) refinement are presented elsewhere (Novais et al., 2011). EXAFS and XEOL experiments were carried out at the D08B:XAFS2 and D04A:SXS beamlines of the Brazilian Synchrotron Light Laboratory (LNLS) in Campinas, SP, Brazil. At the XAFS2 beamline, both the Cd L_1-edge and W L_3-edge were measured. The X-ray photon energy intervals were chosen to be 4000–4600 eV and 10170–10850 eV, respectively. EXAFS data were recorded either in transmission or in fluorescence mode. Ion chambers were used to register I_0, the incident X-ray intensity, as well as I_1, the transmitted intensity. In fluorescence mode the X-ray fluorescence was measured using a 15-element solid-state Ge detector array (Canberra model GL0055S). For each step in excitation energy an XEOL emission spectrum was acquired using a spectrometer (Ocean Optics HR2000). Zero-order (or total) luminescence curves were obtained from the integrated area under the emission spectrum as a function of the excitation energy.

At the SXS beamline the measurements were performed in the 3470–3950 eV energy range, which includes the Cd $L_{2,3}$-edges. The EXAFS spectrum was recorded in total electron yield (TEY) mode, i.e. by specimen current. In this experi-

Table 1
Fitting results obtained for coordination shells surrounding the W ion in the $CdWO_4$ lattice.

N is the coordination number, R is the interatomic distance, ΔR_{XRD} and ΔR_{ch} are the difference between R and that determined from XRD refinement (Novais et al., 2011) and the crystallographic database (Chichagov et al., 1966), respectively, and σ^2 is the Debye–Waller factor.

	N	R (Å)	ΔR_{XRD} (Å)	ΔR_{ch} (Å)	σ^2
O1	2	1.785	−0.093	−0.105	0.006
O2	2	1.856	0.028	0.063	0.001
O2	2	2.141	0.024	−0.066	0.001
W	2	3.262	−0.019	−0.034	0.010
Cd	2	3.535	−0.057	−0.064	0.006
Cd	2	3.656	−0.029	−0.035	0.003

mental set-up the zero-order luminescence was measured using a photomultiplier tube. All signals were normalized to the incident photon flux, I_0, registered by the TEY of a reference aluminium foil. In all cases, XEOL was measured in reflectance mode, so it was not significantly influenced by the different penetration depths of X-rays at the Cd and W edges.

3. Results and discussion

The EXAFS data measured at the W L_3 absorption edge were processed using ATHENA software (Ravel & Newville, 2005). The resulting Fourier transform, as well as its corresponding EXAFS oscillations in k-space (shown in the inset), are presented in Fig. 1. Refinement of the experimental signal, also shown in Fig. 1, was carried out using ARTEMIS software (Ravel & Newville, 2005). The R range was limited up to 4.5 Å and each coordination shell formed by two O or Cd ions was taken separately. Table 1 presents the fitted coordination numbers (N), interatomic distances (R) as well as the Debye–Waller factor (σ^2) obtained during the refinement for the main shells. In this table, ΔR_{XRD} and ΔR_{ch} are the deviation of R determined by EXAFS in the present work, compared with
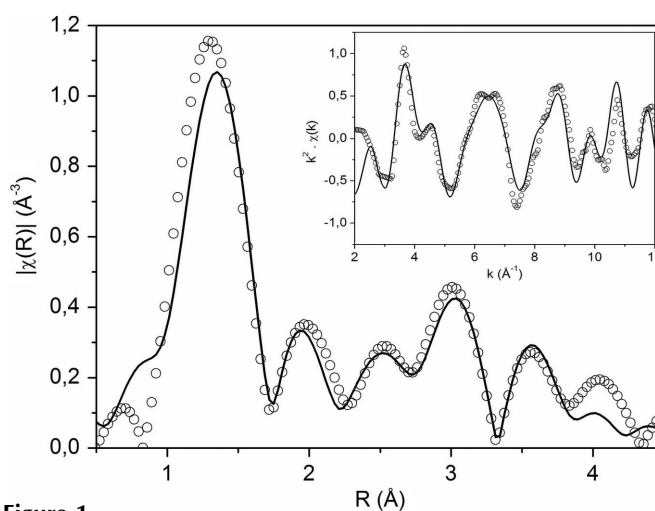

Figure 1
Fourier transform of the EXAFS signal obtained for $CdWO_4$ at the W L_3-edge. The inset shows EXAFS oscillations in k-space. The symbols represent the experimental curves and the solid lines represent the fitting results.

X-ray diffraction from Novais *et al.* (2011) and also with data from the crystallographic database (Chichagov *et al.*, 1966). The results obtained from EXAFS are in good agreement with that obtained by XRD within a deviation lower than 5%, confirming the octahedral symmetry for W. The first W coordination shell is composed of six O ions that can be separated into three distinct pairs at different distances from the central ion. Daturi *et al.* (1997) have determined similar distances through Rietveld analysis of powder XRD patterns and distinguished two types of O atoms in the wolframite structure of $CdWO_4$. One of them (called O1 in Table 1) corresponds to that pair bonded to the W atom with the shorter distance, which gives rise to 'terminal' W—O bonds. Each of this O1 type oxygen is bound to only one W and to two Cd atoms. The second type of O atom (called O2 in Table 1) concerns those pairs connected to the W atom with the longer distances. In this case the oxygen is shared by two W and one Cd atom, such that a chain is formed in the $CdWO_4$ lattice.

Fig. 2 presents XEOL emission spectra of $CdWO_4$ excited by X-rays with energies of 4018 eV (Cd L_1-edge) and 10207 eV (W L_3-edge). The data have been normalized by the maximum intensity (I_{max}) and it is possible to notice that the emission spectrum shape does not depend on the excitation energy. In both curves one can observe the characteristic scintillation of $CdWO_4$, with a broad band emission peaking at 500 nm, which is attributed to the optical transitions within the oxyanionic octahedral WO_6 group (Oosterhout, 1977; Lammers *et al.*, 1981; Mikhailik *et al.*, 2005), and an asymmetry that may be related to the presence of an additional emission band at the long wavelength side of the spectrum. The presence of two emission peaks was previously observed for $CdWO_4$ films excited under 10.21 keV (Shang *et al.*, 2007) and also for UV-excited single crystals (Chirila *et al.*, 2000b). Nevertheless, there is still some debate about the origin of the additional emission in the yellow region. It has been ascribed to transitions in a tungstate group lacking one oxygen ion

(Lammers *et al.*, 1981), and also to the presence of Bi^{3+} impurity (Chirila *et al.*, 2000b). Since the samples used in the present work have a high degree of purity, it is unlikely that Bi^{3+} contamination would be responsible for this second emission band. Additionally, it has been shown by thermally stimulated luminescence measurements that these samples do not contain Bi contamination (see Novais *et al.*, 2011). On the other hand, Hizhnyi *et al.* (2005) have performed computational simulations using the *ab initio* restricted Hartree–Fock method and showed the existence of two types of electronic transitions in WO_6^{6-} groups. Considering the presence of two energetically different O sites in $CdWO_4$ structure, the decay process of the intrinsic tungstate group can occur *via* two slightly different electronic transitions. Therefore, we believe that there is no influence of extrinsic defects on the emission bands observed in Fig. 2.

The inset of Fig. 2 presents the XEOL curves normalized by the intensity of the excitation beam, where it can be observed that the emission intensity for excitation near the W edge was much higher than that measured at the Cd edge. To understand this behavior, it is important to consider the three subprocesses involved in scintillation that affect the XEOL quantum yield (Nikl, 2006; Sham, 2002): (i) X-ray absorption and conversion of the primary excitation into thermalized secondary electronic excitations. The number of secondary excitations is generally very large and strongly depends on the electronic structure of the crystal; (ii) energy transfer toward the luminescent centers, *via* these secondary electronic excitations, promoting them into excited states; (iii) de-excitation of the luminescence centers with emission of optical photons.

In this framework, the XEOL quantum yield can be written as the product of three factors, as shown in equation (1),

$$\eta_{XEOL} = N_{ee}\, S\, Q. \qquad (1)$$

Here, N_{ee} is the number of secondary excitations, which depends on the absorption coefficient, $\mu(E)$, and also characterizes the efficiency of the conversion process. The parameter S refers to the efficiency of energy transfer toward the luminescence centers. The distances over which energy can be transferred will depend on the diffusion length of the electrons (holes) created during the previous step. Secondary electrons and holes (or excitons) may keep their individual mobility or become trapped, either separately or in pairs. At this stage, repeated trapping and energy losses due to non-radiative recombination can occur. Finally, the parameter Q denotes the quantum efficiency of the luminescence centers. As far as one can assume that S and Q do not depend on the energy of the exciting X-ray, Sham (2002) has shown that the XEOL intensity exhibits a linear dependence on the excitation energy and it is also proportional to the total absorptivity of the sample due to the parameter N_{ee}. Taking into account further considerations about the peculiar features of the sample, one may quite reasonable predict the behavior of XEOL excitation spectra.

For $CdWO_4$, since the luminescence centers are located in the WO_6 groups, the secondary excitations created due to Cd absorption can possibly undergo many events such as trapping
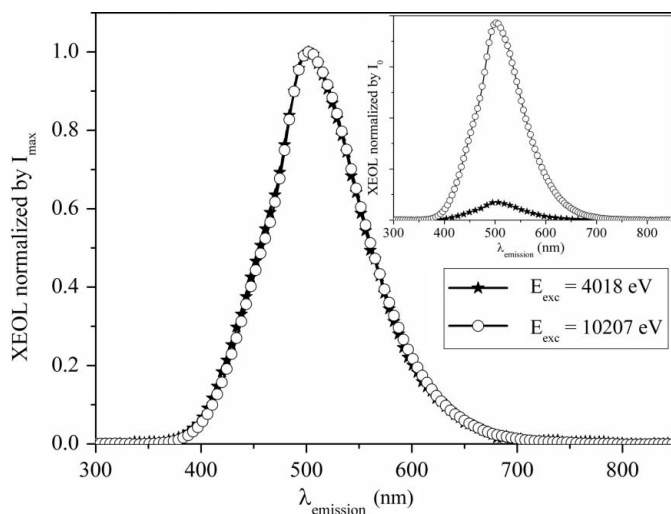

Figure 2
XEOL emission spectra, normalized by the maximum intensity, of $CdWO_4$ powder under excitation at energies near the Cd L_1- and W L_3-edges. The inset shows these spectra normalized by the incident photon flux.

Figure 3
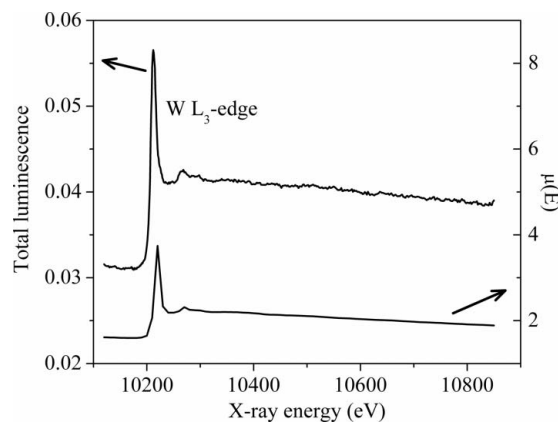XEOL curve in the excitation mode for CdWO$_4$ powder under excitation of X-rays with energies across the W L_3-edge. The EXAFS spectrum was measured in transmission mode and is shown for comparison.

Figure 4
XEOL curve in the excitation mode for CdWO$_4$ powder under excitation of X-rays with energies across the Cd $L_{2,3}$-edges. The EXAFS spectrum was measured in TEY mode and is shown for comparison.

Figure 5
XEOL curve in the excitation mode for CdWO$_4$ powder under excitation of X-rays with energies across the Cd L_1-edge. The EXAFS spectrum was measured in fluorescence mode and is shown for comparison.

and non-radiative decay, thus decreasing the probability of efficient energy transfer to the luminescent centers. The low mobility of these charge carriers may lead to a site selectivity of the excitation, since the parameter S in (1) would be higher for excitation at the W edge.

Fig. 3 presents the XEOL spectrum in the excitation mode, *i.e.* the curve of zero-order luminescence as a function of X-ray excitation energy, for the energy range across the W L_3-edge. The EXAFS spectrum is also presented, for comparison. One observes that the EXAFS spectrum is modulated by the interaction of the outgoing and backscattered waves representing the photoelectron ejected from the W atom. The peaks correspond to the backscattered wave being in phase with the outgoing part while the valleys appear when the two are out of phase (Stern, 1988). The XEOL spectrum presents the same fine structure as the absorption coefficient, $\mu(E)$, meaning that the processes of conversion, transport and luminescence are very efficient when W is the absorbing ion. Electronic structure calculations for CdWO$_4$ have shown that the O $2p$ states dominate the top of the valence band whereas the lower portion of the conduction band derives primarily from the W $5d$ states (Abraham *et al.*, 2000). The most probable secondary electronic excitations formed in the WO$_6$ molecular group after the X-ray absorptions are self-trapped excitons and the intrinsic luminescence of CdWO$_4$ arises due to annihilation of these excitons (Pankratov *et al.*, 2001), so the entire process yielding the XEOL emission observed in Fig. 2 is expected to be localized inside the WO$_6$ group.

XEOL spectra in the excitation mode are presented in Figs. 4 and 5 for the energy range that includes the Cd L-edges. In this case the XEOL curves did not show either the jump or the fine structure observed for the EXAFS over the same energy range, but a steady increase in the total light yield as the excitation energy increased.

Considering the sub-processes involved, the scintillation begins with the creation of secondary excitation owing to the X-ray absorption of Cd states, followed by the energy transfer between the excited Cd and the luminescence centers in the WO$_6$ groups that decay emitting visible light. The possible secondary excitations created with the participation of Cd
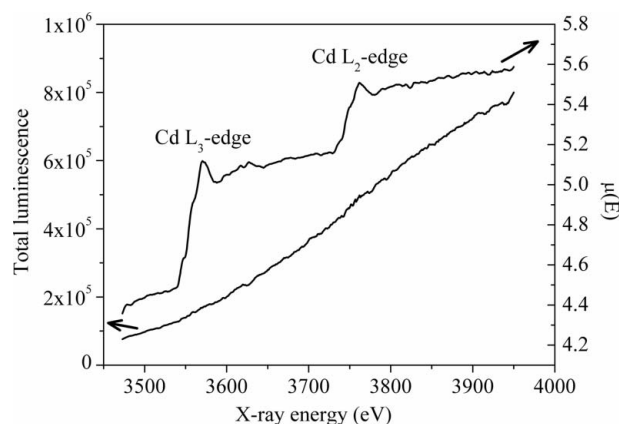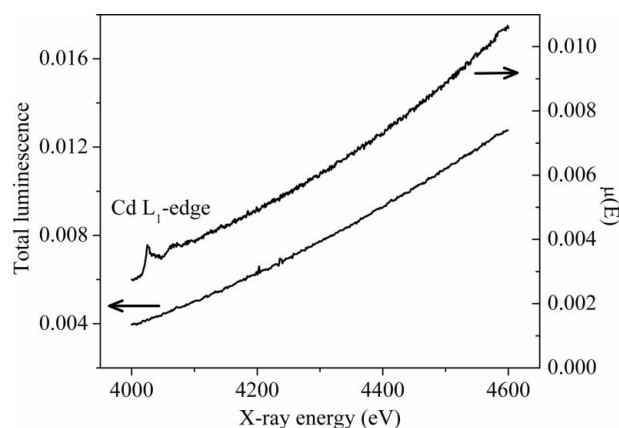
states mentioned in the literature are free electrons (Nagirnyi *et al.*, 2002) and holes that are re-trapped in O$^-$ centers (Laguta *et al.*, 2008; Novais *et al.*, 2011). These charge carriers would eventually migrate through the lattice, be trapped at the WO$_6$ groups, and interact to form trapped excitons. The lower intensity of luminescence under excitation at the Cd edge (see inset of Fig. 2), as well as the lack of correspondence between EXAFS and XEOL (Figs. 4 and 5), is indicative that this process is less effective for luminescence than the direct formation of self-trapped excitons induced by the local excitation of the W ions. The enhancement in the total light yield observed in Figs. 4 and 5 as the excitation energy increases can be associated with the higher kinetic energy of the photoelectrons generated, which enhance their diffusion length and, consequently, the probability of energy transfer to the luminescence centers.

Owing to experimental limitations, the measurements were not extended to the energy range across the oxygen edges, but this investigation should be performed in future works, to clarify the contribution of the core-levels of O ions to the scintillation of CdWO$_4$.

4. Conclusions

Structural and optical properties of $CdWO_4$ polycrystalline samples were studied. EXAFS results confirmed that W ions are surrounded by six O ions and that there are three different lengths for the W—O bonds. The local order, as determined by EXAFS, agrees with the previous results obtained from XRD results.

The selective character of synchrotron radiation helped us to clarify the role played by Cd and W atoms in the scintillation of $CdWO_4$. From the emission spectra, it was possible to notice that the characteristic luminescence of the material is uniquely related to electronic transitions in WO_6 and occurs *via* two slightly different electronic decays, resulting in a main emission at 500 nm and an asymmetry due to an additional luminescence band in the yellow region. The XEOL emission spectra kept the same profile, regardless of the excitation energy of the X-rays photons, and no influence of impurities was detected. The emission of $CdWO_4$ under excitation across the W L_3-edge presented high efficiency and the XEOL excitation spectrum contains the same oscillations of the EXAFS signal. On the other hand, the scintillation measured under excitation near the Cd L-edges was lower and the XEOL excitation spectra did not present the EXAFS fine structure. These results reveal a site-selectivity of the scintillation process in $CdWO_4$, indicating a direct dependence of the light output on the absorption of high-energy photons by the W atoms.

References

Abraham, Y., Holzwarth, N. A. W. & Williams, R. T. (2000). *Phys. Rev. B*, **62**, 1733–1741.

Blasse, G. (1994). *Chem. Mater.* **6**, 1465–1475.

Burachas, S. Ph., Danevich, F. A., Georgadze, A. Sh., Klapdor-Kleingrothaus, H. V., Kobychev, V. V., Kropivyansky, B. N., Kuts, V. N., Muller, A., Muzalevsky, V. V., Nikolaiko, A. S., Ponkratenko, O. A., Ryzhikov, V. D., Sai, A. S., Solsky, I. M., Tretyak, V. I. & Zdesenko, Yu. G. (1996). *Nucl. Instrum. Methods Phys. Res. A*, **369**, 164–168.

Chichagov, A. V., Ilyukhin, V. V. & Belov, N. V. (1966). *Dokl. Akad. Nauk SSSR*, **166**, 87–89.

Chirila, M. M., Garces, N. Y., Murphy, H. J., Wicks, C., Grencewicz, K., Halliburton, L. E. & Giles, N. C. (2000a). *J. Phys. Chem. Solids*, **61**, 1871–1876.

Chirila, M. M., Stevens, K. T., Murphy, H. J. & Giles, N. C. (2000b). *J. Phys. Chem. Solids*, **61**, 675–681.

Daturi, M., Busca, G., Borel, M. M., Leclaire, A. & Piaggio, P. (1997). *J. Phys. Chem. B*, **101**, 4358–4369.

Greskovich, C. & Duclos, S. (1997). *Annu. Rev. Mater. Sci.* **27**, 69–88.

Hizhnyi, Yu. A., Nedilko, S. G. & Nikolaenko, T. N. (2005). *Nucl. Instrum. Methods Phys. Res. A*, **537**, 36–39.

Ko, J. Y., Yiu, Y. M., Liang, H. & Sham, T. K. (2010). *J. Chem. Phys.* **132**, 234701.

Laguta, V. V., Nikl, M., Rosa, J., Grinyov, B. V., Nagornaya, L. L. & Tupitsina, I. A. (2008). *J. Appl. Phys.* **104**, 103525.

Lammers, M. J. J., Blasse, G. & Robertson, D. S. (1981). *Phys. Status Solidi A*, **63**, 569–572.

Liu, L., Chan, J. & Sham, T. K. (2010). *J. Phys. Chem. C*, **114**, 21353–21359.

Mikhailik, V. B., Kraus, H., Miller, G., Mykhaylyk, M. S. & Wahl, D. (2005). *J. Appl. Phys.* **97**, 083523.

Nagirnyi, V., Feldbach, E., Jönsson, L., Kirm, M., Kotlov, A., Lushchik, A., Nagornaya, L. L., Savikhin, F. & Svensson, G. (2001). *Radiat. Meas.* **33**, 601–604.

Nagirnyi, V., Feldbach, E., Jönsson, L., Kirm, M., Kotlov, A., Lushchik, A., Nefedov, V. A. & Zadneprovski, B. I. (2002). *Nucl. Instrum. Methods Phys. Res. A*, **486**, 395–398.

Nagirnyi, V., Kirm, M., Kotlov, A., Lushchik, A. & Jönson, L. (2003). *J. Lumin.* **102–103**, 597–603.

Nikl, M. (2006). *Meas. Sci. Technol.* **17**, R37–R54.

Novais, S. M. V., Silva, R. S. & Macedo, Z. S. (2011). *J. Lumin.* **131**, 1283–1287.

Oosterhout, A. B. (1977). *J. Chem. Phys.* **67**, 2412–2418.

Pankratov, V., Grigorjeva, L., Millers, D., Chernov, S. & Voloshinovskii, A. S. (2001). *J. Lumin.* **94–95**, 427–432.

Ravel, B. & Newville, M. (2005). *J. Synchrotron Rad.* **12**, 537–541.

Rodnyi, P. A. (1997). *Physical Processes in Inorganic Scintillators.* Boca Raton: CRC Press.

Sabharwall, S. C. & Sangeeta (1999). *J. Cryst. Growth*, **200**, 191–198.

Sham, T. K. (2002). *Chemical Applications of Synchrotron Radiation. Part II: X-ray Applications.* Singapore: World Scientific.

Shang, H. M., Bliss, M., Heald, S., Sham, T. K., Heigl, F. & Cao, G. Z. (2007). *J. Mater. Res.* **22**, 1527–1536.

Soderholm, L., Liu, G. K., Antonio, M. R. & Lytle, F. W. (1998). *J. Chem. Phys.* **109**, 6745–6752.

Stern, E. A. (1988). In *X-ray Absorption*, edited by D. C. Koningsberger and R. Prins. New York: Wiley.